In-Plane Critical Magnetic Fields in Magic-Angle Twisted Trilayer Graphene

Wei Qin and Allan H. MacDonald

Phys. Rev. Lett. **127**, 097001 — Published 23 August 2021

DOI: 10.1103/PhysRevLett.127.097001

In-plane critical magnetic fields in magic-angle twisted trilayer graphene

Wei Qin[1] and Allan H. MacDonald[1]

[1] *Department of Physics, The University of Texas at Austin, Austin, Texas 78712,USA**

(Dated: June 22, 2021)

It has recently been shown [1] that superconductivity in magic-angle twisted trilayer graphene survives to in-plane magnetic fields that are well in excess of the Pauli limit, and much stronger than the in-plane critical magnetic fields of magic-angle twisted bilayer graphene. The difference is surprising because twisted bilayers and trilayers both support the magic-angle flat bands thought to be the fountainhead of twisted graphene superconductivity. We show here that the difference in critical magnetic fields can be traced to a $\mathcal{C}_2\mathcal{M}_h$ symmetry in trilayers that survives in-plane magnetic fields, and also relative displacements between top and bottom layers that are not under experimental control at present. An gate electric field breaks the $\mathcal{C}_2\mathcal{M}_h$ symmetry and therefore limits the in-plane critical magnetic field.

Introduction– Superconductivity has been observed in magic-angle twisted bilayer graphene (MATBG) over a broad range of flat-band fillings and electrical screening environments [2–9]. The underlying mechanism responsible for superconductivity in MATBG remains under active debate; both strong electron-electron interaction driven unconventional superconductivity [10–28], and electron-phonon interaction mediated conventional superconductivity [29–33] have been considered theoretically. The recent confirmation of superconductivity in magic-angle twisted trilayer graphene (MATTG) [34–36] represents an important advance because MATTG and MATBG share nearly identical flat bands at twist angles that differ by a factor of $\sqrt{2}$ [37–41], but also have important differences. In particular, the trilayer hosts both even parity flat bands and odd parity dispersive bands that can be mixed by a mirror-symmetry-breaking electric displacement fields [34, 35].

Since the densities of states of MATBG and MATTG are both dominated near neutrality by magic-angle flat bands, it is not surprising that the two systems share many properties, including similar patterns of broken flavor symmetries, and a strong superconducting dome between moiré filling factors $\nu = -2$ and -3 [34, 35]. It is therefore remarkable that MATBG and MATTG superconductors differ qualitatively in their response to in-plane magnetic fields. Whereas the in-plane critical magnetic field is comparable with the Pauli limit in MATBG [42], this limit is exceeded by nearly a factor of three in MATTG [1]. We show below that this surprising observation can be explained if we assume that both systems have valley-singlet spin-triplet Cooper pairs.

Generally speaking, superconductivity is suppressed by magnetic fields because they break the time-reversal ($\mathcal{T}$) symmetry that guarantees degeneracy of the electron pairs that combine to form Cooper-pair bound states. For example, if the Cooper pairs in MATBG and MATTG were spin-singlets, Zeeman splitting Δ_z of opposite spins would suppress superconductivity when the Pauli limit $\Delta_z \approx 1.75 k_B T_c$ is exceeded [43, 44]. In this work we take the view that superconductivity must be nearly identical in MATBG and MATTG. Since the Pauli limit is exceeded in MATTG [1], we conclude that the Cooper pairs must be spin triplets not only in trilayers but also in bilayers. We will see that this view nevertheless provides a natural explanation for the difference in-plane critical fields. Indeed there is some evidence [45–47] that in both systems the state from which superconductivity emerges is a spin polarized ferromagnet [48], leaving spin-triplets as the only pairing possibility.

TABLE I. Symmetries of MATTG models with different attributes (see main text). We distinguish symmetry operations that map electronic states between valleys (intervalley) from those that preserve valley (intravalley). $\mathcal{T}\mathcal{M}_h$ and $\mathcal{C}_2\mathcal{M}_h$ symmetries are equivalent when intravalley $\mathcal{C}_2\mathcal{T}$ symmetry is present. Layer energy refers to the difference between π-orbital energies on interior and exterior layers. Sublattice refers to sublattice polarization within layers.

	Intravalley				Intervalley		
	$\mathcal{C}_3$	$\mathcal{M}_h$	$\mathcal{C}_2\mathcal{T}$	$\mathcal{C}_2\mathcal{T}\mathcal{M}_h$	$\mathcal{T}$	$\mathcal{T}\mathcal{M}_h$	$\mathcal{C}_2\mathcal{M}_h$
Layer energy	✓	✓	✓	✓	✓	✓	✓
Gate field	✓	×	✓	×	✓	×	×
Lateral shift	×	×	×	✓	✓	×	✓
In-plane $\boldsymbol{B}_{\|\|}$	×	×	✓	×	×	✓	✓
Sublattice	✓	✓	×	×	✓	✓	×

In the absence of a magnetic field, $\mathcal{T}$ symmetry guarantees that band states with opposite momentum in opposite valleys are degenerate. These are the states that pair in valley-singlet superconductors. In-plane magnetic field $\boldsymbol{B}_{||}$ breaks $\mathcal{T}$ symmetry in both bilayers and trilayer. In bilayers this produces an energy splitting that suppresses superconductivity [42, 49]. In trilayers, however, both time-reversal and mirror ($\mathcal{T}\mathcal{M}_h$) and twofold rotation and mirror ($\mathcal{C}_2\mathcal{M}_h$) symmetries survive (see Table I) and, as we explain below, independently guarantee the degeneracy that supports valley-singlet superconductivity. In Fig. 1, we illustrate this qualitative difference by comparing typical Fermi surfaces of MATBG and MATTG at finite $\boldsymbol{B}_{||}$.

Below we first confirm this symmetry argument by per-

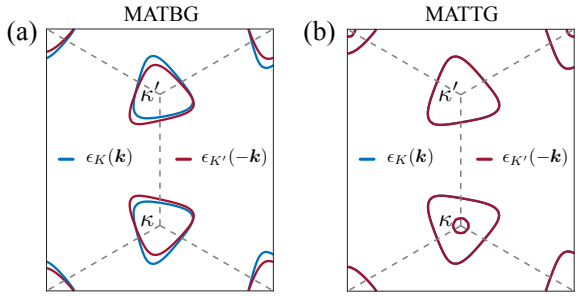

FIG. 1. Nesting between $\epsilon_K(\boldsymbol{k})$ and $\epsilon_{K'}(-\boldsymbol{k})$ Fermi surfaces for in-plane magnetic field $B_x = 2$ T and moiré filling factor $\nu = -2.4$ in (a) MATBG and (b) MATTG. In (a), $\epsilon_K(\boldsymbol{k}) \neq \epsilon_{K'}(-\boldsymbol{k})$ due to broken $\mathcal{T}$ symmetry. In (b), $\epsilon_K(\boldsymbol{k}) = \epsilon_{K'}(-\boldsymbol{k})$ survives because this degeneracy is guaranteed by $\mathcal{C}_2\mathcal{M}_h$ symmetry, which survives in-plane magnetic fields as summarized in Table. I. The small Fermi pocket around the κ point is contributed by dispersive Dirac bands, which are centered on κ and κ' in the K and K' valleys, respectively. Since we plot $\epsilon_{K'}(-\boldsymbol{k})$, both pockets are κ-centered.

forming mean-field calculations of $\boldsymbol{B}_{||}$ dependent superconducting critical temperatures, using continuum model band structures and a phenomenological attractive interaction. We then study the influence on the in-plane critical magnetic field of gate electric fields, which can easily be tuned experimentally, and lateral shifts of the top or bottom graphene layer, which may occur accidentally. We find that the former breaks both $\mathcal{T}\mathcal{M}_h$ and $\mathcal{C}_2\mathcal{M}_h$ symmetries, leading to a reduced in-plane critical magnetic field, while the later preserves $\mathcal{C}_2\mathcal{M}_h$ symmetry thereby retaining state degeneracy and robust superconductivity.

Band structure and symmetries — An approximate single-particle band structure model of MATTG can be constructed by generalizing the Bistritzer-MacDonald MATBG model [50]. In the absence of gate electric fields and lateral shifts, the K-valley projected Hamiltonian

$$\mathcal{H}_K = \begin{bmatrix} h_{\theta/2}(\boldsymbol{k}) & T(\boldsymbol{r}) & 0 \\ T^\dagger(\boldsymbol{r}) & h_{-\theta/2}(\boldsymbol{k}) & T^\dagger(\boldsymbol{r}) \\ 0 & T(\boldsymbol{r}) & h_{\theta/2}(\boldsymbol{k}) \end{bmatrix}, \tag{1}$$

where $h_\theta(\boldsymbol{k}) = e^{i\frac{i\theta}{2}\sigma_z}(v_D\boldsymbol{k}\cdot\boldsymbol{\sigma})e^{-i\frac{\theta}{2}\sigma_z}$, v_D is the Dirac velocity of isolated monolayer graphene, and $\boldsymbol{\sigma} = (\sigma_x, \sigma_y)$ are Pauli matrices acting on sublattice. The interlayer tunneling matrix $T(\boldsymbol{r}) = \sum_{n=1}^{3} T_n e^{i\boldsymbol{q}_n\cdot\boldsymbol{r}}$, where $T_{n+1} = t_{\rm AA}\sigma_0 + t_{\rm AB}[\cos(n\phi)\sigma_x + \sin(n\phi)\sigma_y]$ and $\phi = 2\pi/3$. It follows from mirror symmetry that $\mathcal{H}_K$ can be written in a representation of decoupled even-parity and odd-parity states [39, 40]. From Eq. (1), we see that the trilayer's even parity subspace Hamiltonian maps to that of a bilayer, with the even parity combination of the trilayer's outer layers playing the role of a single layer. Because two different tunneling terms couple the inside and outside layers, the effective bilayer tunneling amplitude, (and therefore the magic twist angle, the flat band width, and the density of states) increases by a factor of $\sqrt{2}$. The odd parity band, also formed from the outside layers, is identical to that of an isolated graphene layer and strongly dispersive [39, 40].

Although Eq. (1) captures the essential properties of MATTG, some modifications that we classify in Table I can be important. First, since the chemical environments of the middle and outer graphene layers in MATTG are different, there is a layer energy difference between them [41], which does not break any symmetry. Other modifications break one or more of the $\mathcal{T}$, $\mathcal{C}_3$, $\mathcal{M}_h$, $\mathcal{C}_2\mathcal{T}$, and $\mathcal{C}_2\mathcal{M}_h\mathcal{T}$ symmetries of undisturbed trilayers. For example, the electric fields routinely applied using gates break $\mathcal{M}_h$ symmetry and hybridize the dispersive Dirac bands and flat bands. Because $\mathcal{C}_3$ and $\mathcal{C}_2\mathcal{T}$ symmetries survive this perturbation, gapless Dirac cones remain at the κ and κ' points of the moiré Brillouin zone (MBZ) [39–41]. Additionally, relative translational shifts between the top and bottom graphene layers, which are not under experimental control at present, can occur even though first-principles calculations show that the mirror symmetric configuration is energetically most stable [39]. Lateral shifts can be captured by adding phase factors to $T(\boldsymbol{r})$ [50] and break $\mathcal{C}_3$, $\mathcal{M}_h$ and $\mathcal{C}_2\mathcal{T}$ symmetries. The gapless Dirac cones nevertheless remain because they are protected by $\mathcal{C}_2\mathcal{T}\mathcal{M}_h$ symmetry, and simply move away from κ and κ' points. Table I summarizes these symmetry considerations.

In-plane magnetic fields — The application of $\boldsymbol{B}_{||}$ to MATBG or MATTG induces a layer-dependent gauge field $\boldsymbol{A}_l = \boldsymbol{B}_{||} \times \boldsymbol{z}_l$ [49, 51]. For MATBG, the gauge field shifts the momenta of electrons in the the top and bottom graphene layers along opposite directions so that

$$\mathcal{H}_K(\boldsymbol{k}) = \begin{bmatrix} h_{\theta/2}(\boldsymbol{k}+\boldsymbol{p}/2) & T(\boldsymbol{r}) \\ T^\dagger(\boldsymbol{r}) & h_{-\theta/2}(\boldsymbol{k}-\boldsymbol{p}/2) \end{bmatrix}, \tag{2}$$

where $\boldsymbol{p} = (\pi d/\Phi_0)(B_y, -B_x)$, d is the interlayer distance, Φ_0 denotes the magnetic flux quantum, and we have placed $z = 0$ at the center of the two layers. Since the momenta of the electrons from the same layer but in opposite valleys are shifted along the same direction, $\mathcal{T}$ symmetry is broken, and $\delta E \equiv \epsilon_{K'}(-\boldsymbol{k}) - \epsilon_K(\boldsymbol{k}) \neq 0$ as illustrated in Fig. 1(a), suppressing contributions to valley singlet ladder sums. Therefore, the application of $\boldsymbol{B}_{||}$ leads to a reduction on the superconducting critical temperature T_c. The critical magnetic field B_c at which T_c is driven to zero is reached when $\delta E \sim \Delta$, where Δ is the gap in the absence of $\boldsymbol{B}_{||}$.

In the MATTG case, choosing $z = 0$ in the middle layer, the gauge field shifts momenta of top and bottom layer electrons along opposite directions, while leaving the middle graphene layer unaffected. The K-valley

Hamiltonian

$$\mathcal{H}_K(\boldsymbol{k}) = \begin{bmatrix} h_{\theta/2}(\boldsymbol{k}+\boldsymbol{p}) & T(\boldsymbol{r}) & 0 \\ T^\dagger(\boldsymbol{r}) & h_{-\theta/2}(\boldsymbol{k}) & T^\dagger(\boldsymbol{r}) \\ 0 & T(\boldsymbol{r}) & h_{\theta/2}(\boldsymbol{k}-\boldsymbol{p}) \end{bmatrix}, \quad (3)$$

has broken $\mathcal{C}_3$ and $\mathcal{M}_h$ symmetries. Note that the sign of $\boldsymbol{p}$ is changed by a miror operation. Although $\mathcal{T}$ symmetry is broken, the two valleys can still be mapped to each other by either the combined $\mathcal{C}_2\mathcal{M}_h$ or $\mathcal{T}\mathcal{M}_h$ symmetry, as summarized in Table I. Therefore, $\epsilon_{K'}(-\boldsymbol{k}) = \epsilon_K(\boldsymbol{k})$ even in the presence of $\boldsymbol{B}_{||}$, suggesting a perfect intervalley Fermi surface nesting as shown in Fig. 1(b). Because the quasiparticle pairs from which the Cooper pairs are formed retain degeneracy there is no obvious mechanism to suppress superconductivity. Indeed, numerical model calculations summarized below suggest that superconductivity in MATTG can survive at extremely large values of $\boldsymbol{B}_{||}$. On the other hand simultaneous breaking of $\mathcal{C}_2\mathcal{M}_h$ and $\mathcal{T}\mathcal{M}_h$ symmetries by an gate electric field, lifts the pairing degeneracy and leads to a reduced B_c.

Numerical model calculations — Superconductivity occurs in MATBG and MATTG when each is close to its magic rotation angle. We therefore compare the two systems with $\theta_{\rm TBG} = 1.1^\circ$ and $\theta_{\rm TTG} = \sqrt{2} \times 1.1^\circ$. First principles calculations show that the moiré patterns of both systems distort to avoid high energy local AA stacking, leading to $t_{\rm AA}/t_{\rm AB} < 1$ [39, 52]. Here we take $t_{\rm AA}/t_{\rm AB} = 0.7$ for both systems. Similarly, particle-hole asymmetric behavior has also been observed in the transport measurements of MATTG [34, 35], and becomes dramatic near the magic angle. This property can be modeled by including a nonlocal momentum-dependent correction to interlayer tunneling [45]. We choose $dt_{\rm AA}/dk = dt_{\rm AB}/dk = -0.1$ in this study. The nonlocal interlayer tunneling also increases the energy difference between the dispersive Dirac bands and the flat bands of MATTG. Below, the moiré filling factor is fixed at $\nu = -2.4$, where the experimentally observed T_c is commonly maximized in both MATBG and MATTG superconductors [2–4, 34, 35]. As discussed in the introduction, we take the view that the normal state at $\nu = -2.4$ is spin polarized due to flavor symmetry breaking [46]. In the model we study, the Fermi surfaces are located around the κ and κ' points of MBZ as shown in Fig. 1. This detail is not yet established experimentally.

We perform mean-field Bogoliubov-de Gennes calculations that account for $\boldsymbol{B}_{||}$ to determine T_c and B_c. Our calculations employ a model interaction Hamiltonian

$$\begin{aligned} H_{int} = U \sum_{l\sigma} \int d\boldsymbol{r} \psi^\dagger_{+l\sigma}(\boldsymbol{r}) \psi^\dagger_{-l\sigma}(\boldsymbol{r}) \psi_{-l\sigma}(\boldsymbol{r}) \psi_{+l\sigma}(\boldsymbol{r}) \\ + V \sum_{l\sigma} \int d\boldsymbol{r} \psi^\dagger_{+l\sigma}(\boldsymbol{r}) \psi^\dagger_{-l\bar{\sigma}}(\boldsymbol{r}) \psi_{-l\bar{\sigma}}(\boldsymbol{r}) \psi_{+l\sigma}(\boldsymbol{r}), \end{aligned} \quad (4)$$

where $\pm$, l, and σ are valley, layer, and sublattice indices, respectively. The intra- (U) and inter-sublattice (V) interacting strengths can have important screened Coulomb [28, 53, 54], electron-phonon mediated [29–31, 55], and flavor-fluctuation-mediated interaction contributions [47, 56]. In the absence of a microscopic theory, we approximate U and V as momentum-independent tunable parameters that support valley-singlet spin-triplet pairing [57, 58]. Our illustrative calculations use $U = -320$ meV·nm^2 and $V = 480$ meV·nm^2. This choice yields $T_c \sim 2$ K, comparable with experimental observations [34, 35], in the absence of $\boldsymbol{B}_{||}$. No qualitative aspect of our results depends on this model choice provided that pairing occurs between electrons from opposite valleys with the same spin.

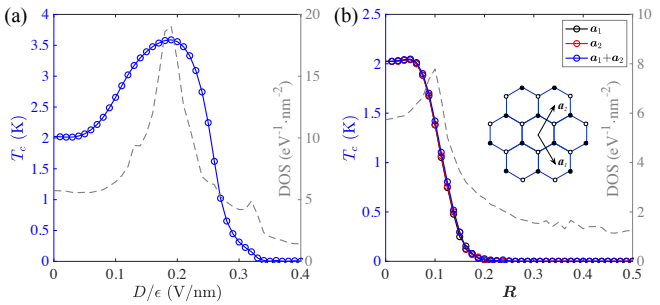

FIG. 2. (a) MATTG mean-field T_c *vs.* gate electric field D/ϵ. The dashed curve shows the Fermi-level density of states. (b) T_c *vs.* lateral shift $\boldsymbol{R}$ of the top or bottom graphene layer. The insert defines the directions of the lateral shift relative to the lattice vectors of the shifted graphene layer. The dashed curve again plots the Fermi level density of states.

Critical temperature — Figure 2(a) shows the MATTG mean-field T_c as a function of the screened gate electric field D/ϵ. We find that a maximum in T_c is reached at an intermediate value of $D/\epsilon \sim 0.19$ V/nm, after which T_c drops, vanishing at $D/\epsilon \sim 0.34$ V/nm. The dome-like behavior of T_c *vs.* D/ϵ is due to the change of density of states (DOS), which is non-monotonic but has a tendency to decrease as D/ϵ and the mixing between even and odd parity bands it produces increase. In Fig. 2(a), the peak of the DOS coincides with the maximum value of T_c. The dome-like behavior agrees qualitatively with recent experimental observations of T_c in MATTG [34, 35], indicating that DOS variations likely play a role. Figure 2(b) illustrates the effect of a lateral shift $\boldsymbol{R}$ of the top or bottom graphene layer on T_c. Superconductivity is completely suppressed when $\boldsymbol{R} \sim 0.2\boldsymbol{a}$ with $\boldsymbol{a}$ the lattice vector of the shifted graphene layer. The suppression of T_c is almost isotropic and caused by a dramatic reduction of DOS at sufficiently large lateral shift where the flat bands become more dispersive due to $\mathcal{M}_h$ symmetry breaking. The fact that the critical temperatures are similar in MATTB and MATBG may indicate that $\boldsymbol{R}$ is small in experimental devices due to energy minimization.

In-plane critical magnetic field — Figure 3(a) shows

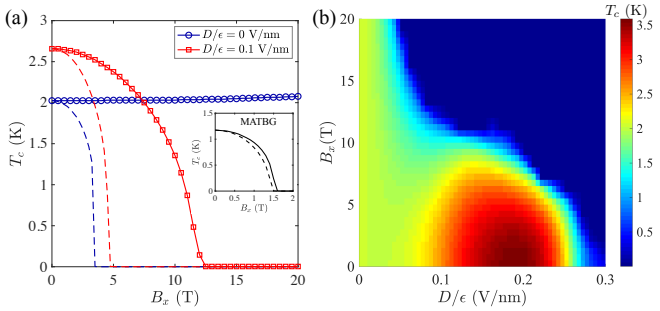

FIG. 3. (a) Mean-field T_c *vs.* in-plane magnetic field applied along x direction B_x for MATTG with valley-singlet spin-triplet pairing at zero and finite gate electric field D/ϵ. The insert plots T_c as function of B_x for MATBG. The dashed curves plot similar results for valley-triplet spin-singlet pairing. (b) Two-dimensional color plot of T_c *vs.* B_x and D/ϵ for MATTG . These results are calculated with $\boldsymbol{R} = 0$.

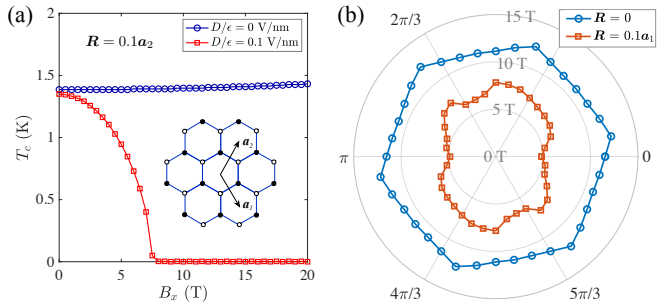

FIG. 4. (a) T_c *vs.* B_x and D/ϵ at a lateral shift $\boldsymbol{R} = 0.1\boldsymbol{a}_2$. (b) Angular dependence of B_c for zero ($\boldsymbol{R} = 0$) and finite ($\boldsymbol{R} = 0.1\boldsymbol{a}_1$) lateral shifts of the top or bottom graphene layer. In (b) we chose $D/\epsilon = 0.1$ V/nm.

valley-singlet spin-triplet critical temperatures T_c calculated at finite values of $\boldsymbol{B}_{||}$, and compares with the case of valley-triplet spin-singlet pairing for which Zeeman coupling plays a role. As illustrated in the insert of Fig. 3(a), breaking $\mathcal{T}$ symmetry by applying B_x dramatically suppresses T_c in MATBG for both of spin-singlet and spin-triplet pairing. The in-plane critical magnetic field obtained for MATBG superconductors is $B_c \sim 1.6$ T, which is consistent with experimental observations [42]. Because B_c for spin-singlet and spin-triplet pairing is nearly the same in MATBG, the $\boldsymbol{B}_{||}$ response does not clearly distinguish spin-singlet pairing from spin-triplet pairing. In MATTG, on the other hand, $\mathcal{C}_2\mathcal{M}_h$ or $\mathcal{T}\mathcal{M}_h$ symmetry survives $\boldsymbol{B}_{||}$, resulting in an infinite large B_c for spin-triplet pairing at $D/\epsilon = 0$ V/nm as illustrated in Fig. 3(a). The small increase in T_c is attributed to the change of the DOS in the presence of B_x. Application of a gate electric field to MATTG breaks both of $\mathcal{C}_2\mathcal{M}_h$ and $\mathcal{T}\mathcal{M}_h$ symmetries, as summarized in Table I, leading to the suppression on T_c at finite values of B_x shown in Fig. 3(a). For $D/\epsilon = 0.1$ V/nm, $B_c \sim 12$ T, well in excess of the the Pauli limit estimated by $B_P \approx 1.86 T_c \approx 4.8$ T. In comparison to spin-triplet pairing, T_c for spin-singlet pairing is strongly suppressed by B_x as shown in Fig. 3(a). The critical in-plane magnetic field for $D/\epsilon = 0$ V/nm and $D/\epsilon = 0.1$ V/nm are 3.5 T and 4.75 T, which are consistent with the corresponding Pauli limits, indicating that the Zeeman effect dominants the pairing breaking for spin-singlet pairing in MATTG. Because orbital pair breaking by B_x is weak at small values of D/ϵ, studies of T_c *vs.* B_x clearly distinguish spin-singlet and spin-triplet superconductivity in MATTG [1]. Figure 3(b) shows T_c *vs.* B_x and D/ϵ, illustrating the robustness of superconductivity at finite B_x when D/ϵ is small.

Figure 4(a) illustrates the influence of the lateral shift of top or bottom graphene layer on T_c at finite values of B_x. As summarized in Table.I, although $\mathcal{T}\mathcal{M}_h$ symmetry is broken by lateral shifts, the $\mathcal{C}_2\mathcal{M}_h$ symmetry survives. The critical magnetic field is therefore infinite at $D/\epsilon = 0$ V/nm and large at small values of D/ϵ. In our model calculations $B_c \sim 8$ T for $D/\epsilon = 0.1$ V/nm. Figure 4(b) shows the angle-dependence of B_c for $D/\epsilon = 0.1$ V/nm. Note that in the absence of lateral shift, B_c has a sixfold rotation symmetry for valley-singlet pairing, even though each valley possesses only $\mathcal{C}_3$ symmetry. A lateral shift of the top or bottom graphene layer breaks $\mathcal{C}_3$ symmetry and suppresses T_c as shown in Fig. 2(b), resulting in a reduced B_c with twofold rotation symmetry, as illustrated in Fig. 4(b).

Discussion — The present study provides an explanation for the recent observation of extremely large in-plane critical magnetic field in MATTG superconductors [1] by relating it to a $\mathcal{C}_2\mathcal{M}_h$ symmetry that survives both $\boldsymbol{B}_{||}$ and relative lateral shifts of one of the outside graphene layers. $\mathcal{C}_2\mathcal{M}_h$ symmetry is broken by gate electric fields. By combining model band structures with phenomenological electron-electron interactions, we obtain values for T_c at finite $\boldsymbol{B}_{||}$ that agree qualitatively with experimental observations, and provide an explanation for the partially contrasting properties of MATBG and MATTG superconductors that is consistent provided that both have valley-singlet spin-triplet pairing.

In our theory we find that in the absence of a gate electric fields there is practically no suppression of superconductivity by $\boldsymbol{B}_{||}$, whereas the experimental critical fields are finite. We attribute the supression of superconductivity in experiment to $\mathcal{M}_h$ symmetry-breaking disorder that is always present in experimental devices, due for example to spatially random vertical electric fields. Another likely culprit is random differences between the local twist angle between the top and middle graphene layers and the local twist angle between the bottom and middle graphene layers [35, 59]. Both potential and twist-angle disorders generically break $\mathcal{M}_h$ symmetry and will lead to a finite B_c even if spatially averaged potentials and twist angles preserve this symmetry. Finally, $\mathcal{C}_2\mathcal{T}$

symmetry breaking due to Fock self-energies, thought to occur in the insulating state at $\nu = -2$ [45, 60], would if present suppress superconductivity at $D/\epsilon = 0$ V/nm for $\boldsymbol{R} \neq 0$, as indicated in Table I. It follows from our analysis that measurements of B_c anisotropy can be used to identify $\boldsymbol{R} \neq 0$ devices, and in this way help identify which of these weak supression mechanisms is active.

The model we employ in this work yield a Fermi surface for $\nu = -2.4$ that has two hole pockets centered on κ and κ' points of the MBZ. The true character of the Fermi surface underlying the superconducting dome is however highly uncertain at present in both MATBG and MATTG because a combination of weak single-particle dispersion and wavefunctions that vary qualitatively with momentum means that mean-field interaction effects are likely to alter band dispersion and Fermi surface topology [61, 62]. At the mean-field level, the Hartree self energies at negative filling factors shift the bands around κ and κ' to lower energies relative to bands around γ as the valence band is emptied, providing a potential opening for hole pocket centered on γ. These electronic structure uncertainties do not alter our main conclusions.

Acknowledgment — The authors acknowledge helpful discussions with M. Xie, C. L. Huang, E. Lake, T. Senthil, and E. Khalaf. This work was supported by DOE grant DE-FG02-02ER45958. Numerical calculations were performed using supercomputing resources at the Texas Advanced Computing Center (TACC).

Note added — A closely related theoretical preprint [63] that focuses on the reentrant superconducting phase observed in MATTG appeared simultaneously with a preprint of this MS.

* macd@physics.utexas.edu

[1] Y. Cao, J. M. Park, K. Watanabe, T. Taniguchi, and P. Jarillo-Herrero, Large Pauli limit violation and reentrant superconductivity in magic-angle twisted trilayer graphene, arXiv:2103.12083 (2021).

[2] Y. Cao, V. Fatemi, S. Fang, K. Watanabe, T. Taniguchi, E. Kaxiras, and P. Jarillo-Herrero, Unconventional superconductivity in magic-angle graphene superlattices, Nature **556**, 43 (2018).

[3] M. Yankowitz, S. Chen, H. Polshyn, Y. Zhang, K. Watanabe, T. Taniguchi, D. Graf, A. F. Young, and C. R. Dean, Tuning superconductivity in twisted bilayer graphene, Science **363**, 1059 (2019).

[4] X. Lu, P. Stepanov, W. Yang, M. Xie, M. A. Aamir, I. Das, C. Urgell, K. Watanabe, T. Taniguchi, G. Zhang, A. Bachtold, A. H. MacDonald, and D. K. Efetov, Superconductors, orbital magnets and correlated states in magic-angle bilayer graphene, Nature **574**, 653 (2019).

[5] L. Balents, C. R. Dean, D. K. Efetov, and A. F. Young, Superconductivity and strong correlations in moiré flat bands, Nature Physics **16**, 725 (2020).

[6] P. Stepanov, I. Das, X. Lu, A. Fahimniya, K. Watanabe, T. Taniguchi, F. H. L. Koppens, J. Lischner, L. Levitov, and D. K. Efetov, Untying the insulating and superconducting orders in magic-angle graphene, Nature **583**, 375 (2020).

[7] Y. Saito, J. Ge, K. Watanabe, T. Taniguchi, and A. F. Young, Independent superconductors and correlated insulators in twisted bilayer graphene, Nature Physics **16**, 926 (2020).

[8] P. Stepanov, M. Xie, T. Taniguchi, K. Watanabe, X. Lu, A. H. MacDonald, B. A. Bernevig, and D. K. Efetov, Competing zero-field Chern insulators in superconducting twisted bilayer graphene, arXiv:2012.15126.

[9] X. Liu, Z. Wang, K. Watanabe, T. Taniguchi, O. Vafek, and J. I. A. Li, Tuning electron correlation in magic-angle twisted bilayer graphene using Coulomb screening, Science **371**, 1261 (2021).

[10] H. Guo, X. Zhu, S. Feng, and R. T. Scalettar, Pairing symmetry of interacting fermions on a twisted bilayer graphene superlattice, Phys. Rev. B **97**, 235453 (2018).

[11] J. F. Dodaro, S. A. Kivelson, Y. Schattner, X. Q. Sun, and C. Wang, Phases of a phenomenological model of twisted bilayer graphene, Phys. Rev. B **98**, 075154 (2018).

[12] C.-C. Liu, L.-D. Zhang, W.-Q. Chen, and F. Yang, Chiral spin density wave and $d + id$ superconductivity in the magic-angle-twisted bilayer graphene, Phys. Rev. Lett. **121**, 217001 (2018).

[13] H. Isobe, N. F. Q. Yuan, and L. Fu, Unconventional superconductivity and density waves in twisted bilayer graphene, Phys. Rev. X **8**, 041041 (2018).

[14] M. Fidrysiak, M. Zegrodnik, and J. Spałek, Unconventional topological superconductivity and phase diagram for an effective two-orbital model as applied to twisted bilayer graphene, Phys. Rev. B **98**, 085436 (2018).

[15] D. M. Kennes, J. Lischner, and C. Karrasch, Strong correlations and $d + id$ superconductivity in twisted bilayer graphene, Phys. Rev. B **98**, 241407(R) (2018).

[16] Y. Sherkunov and J. J. Betouras, Electronic phases in twisted bilayer graphene at magic angles as a result of Van Hove singularities and interactions, Phys. Rev. B **98**, 205151 (2018).

[17] Y. Xie, B. Lian, B. Jäck, X. Liu, C.-L. Chiu, K. Watanabe, T. Taniguchi, B. A. Bernevig, and A. Yazdani, Spectroscopic signatures of many-body correlations in magic-angle twisted bilayer graphene, Nature **572**, 101 (2019).

[18] A. Kerelsky, L. J. McGilly, D. M. Kennes, L. Xian, M. Yankowitz, S. Chen, K. Watanabe, T. Taniguchi, J. Hone, C. Dean, A. Rubio, and A. N. Pasupathy, Maximized electron interactions at the magic angle in twisted bilayer graphene, Nature **572**, 95 (2019).

[19] Y. Choi, J. Kemmer, Y. Peng, A. Thomson, H. Arora, R. Polski, Y. Zhang, H. Ren, J. Alicea, G. Refael, F. von Oppen, K. Watanabe, T. Taniguchi, and S. Nadj-Perge, Electronic correlations in twisted bilayer graphene near the magic angle, Nature Physics **15**, 1174 (2019).

[20] Y. Jiang, X. Lai, K. Watanabe, T. Taniguchi, K. Haule, J. Mao, and E. Y. Andrei, Charge order and broken rotational symmetry in magic-angle twisted bilayer graphene, Nature **573**, 91 (2019).

[21] J. González and T. Stauber, Kohn-Luttinger superconductivity in twisted bilayer graphene, Phys. Rev. Lett. **122**, 026801 (2019).

[22] B. Roy and V. Juričić, Unconventional superconductivity in nearly flat bands in twisted bilayer graphene, Phys. Rev. B **99**, 121407(R) (2019).

[23] T. Huang, L. Zhang, and T. Ma, Antiferromagnetically ordered Mott insulator and $d + id$ superconductivity in twisted bilayer graphene: a quantum Monte Carlo study, Science Bulletin **64**, 310 (2019).

[24] S. Ray, J. Jung, and T. Das, Wannier pairs in superconducting twisted bilayer graphene and related systems, Phys. Rev. B **99**, 134515 (2019).

[25] Y.-Z. You and A. Vishwanath, Superconductivity from valley fluctuations and approximate SO(4) symmetry in a weak coupling theory of twisted bilayer graphene, npj Quantum Materials **4**, 16 (2019).

[26] E. Khalaf, S. Chatterjee, N. Bultinck, M. P. Zaletel, and A. Vishwanath, Charged skyrmions and topological origin of superconductivity in magic angle graphene, arXiv:2004.00638.

[27] W. Qin, B. Zou, and A. H. MacDonald, Critical magnetic fields and electron-pairing in magic-angle twisted bilayer graphene, arXiv:2102.10504 (2021).

[28] T. Cea and F. Guinea, Coulomb interaction, phonons, and superconductivity in twisted bilayer graphene, arXiv:2103.01815 (2021).

[29] F. Wu, A. H. MacDonald, and I. Martin, Theory of phonon-mediated superconductivity in twisted bilayer graphene, Phys. Rev. Lett. **121**, 257001 (2018).

[30] Y. W. Choi and H. J. Choi, Strong electron-phonon coupling, electron-hole asymmetry, and nonadiabaticity in magic-angle twisted bilayer graphene, Phys. Rev. B **98**, 241412(R) (2018).

[31] B. Lian, Z. Wang, and B. A. Bernevig, Twisted bilayer graphene: a phonon-driven superconductor, Phys. Rev. Lett. **122**, 257002 (2019).

[32] M. Angeli, E. Tosatti, and M. Fabrizio, Valley Jahn-Teller effect in twisted bilayer graphene, Phys. Rev. X **9**, 041010 (2019).

[33] C. Lewandowski, S. Nadj-Perge, and D. Chowdhury, Does filling-dependent band renormalization aid pairing in twisted bilayer graphene, arXiv:2102.05661 (2021).

[34] J. M. Park, Y. Cao, K. Watanabe, T. Taniguchi, and P. Jarillo-Herrero, Tunable strongly coupled superconductivity in magic-angle twisted trilayer graphene, Nature **590**, 249 (2021).

[35] Z. Hao, A. M. Zimmerman, P. Ledwith, E. Khalaf, D. H. Najafabadi, K. Watanabe, T. Taniguchi, A. Vishwanath, and P. Kim, Electric fieldtunable superconductivity in alternating-twist magic-angle trilayer graphene, Science **371**, 1133 (2021).

[36] K.-T. Tsai, X. Zhang, Z. Zhu, Y. Luo, S. Carr, M. Luskin, E. Kaxiras, and K. Wang, Correlated insulating states and transport signature of superconductivity in twisted trilayer graphene moiré of moiré superlattices, arXiv:1912.03375 (2019).

[37] E. Khalaf, A. J. Kruchkov, G. Tarnopolsky, and A. Vishwanath, Magic angle hierarchy in twisted graphene multilayers, Phys. Rev. B **100**, 085109 (2019).

[38] C. Mora, N. Regnault, and B. A. Bernevig, Flatbands and perfect metal in trilayer moiré graphene, Phys. Rev. Lett. **123**, 026402 (2019).

[39] S. Carr, C. Li, Z. Zhu, E. Kaxiras, S. Sachdev, and A. Kruchkov, Ultraheavy and ultrarelativistic Dirac quasiparticles in sandwiched graphenes, Nano letters **20**, 3030 (2020).

[40] Z. Zhu, S. Carr, D. Massatt, M. Luskin, and E. Kaxiras, Twisted trilayer graphene: a precisely tunable platform for correlated electrons, Phys. Rev. Lett. **125**, 116404 (2020).

[41] C. Lei, L. Linhart, W. Qin, F. Libisch, and A. H. MacDonald, Mirror symmetry breaking and lateral stacking shifts in twisted trilayer graphene, arXiv:2010.05787 (2020).

[42] Y. Cao, D. Rodan-Legrain, J. M. Park, N. F. Yuan, K. Watanabe, T. Taniguchi, R. M. Fernandes, L. Fu, and P. Jarillo-Herrero, Nematicity and competing orders in superconducting magic-angle graphene, Science **372**, 264 (2021).

[43] B. S. Chandrasekhar, A note on the maximum critical field of high-field superconductor, Applied Physics Letters **1**, 7 (1962).

[44] A. M. Clogston, Upper limit for the critical field in hard superconductors, Phys. Rev. Lett. **9**, 266 (1962).

[45] M. Xie and A. H. MacDonald, Weak-field hall resistivity and spin/valley flavor symmetry breaking in MAtBG, arXiv:2010.07928.

[46] P. Potasz, M. Xie, and A. H. MacDonald, Exact diagonalization for magic-angle twisted bilayer graphene, arXiv:2102.02256 (2021).

[47] A. Fischer, Z. A. Goodwin, A. A. Mostofi, J. Lischner, D. M. Kennes, and L. Klebl, Unconventional superconductivity in magic-angle twisted trilayer graphene, arXiv:2104.10176 (2021).

[48] Superconductors that arise from pairing instabilities of fully spin-polarized normal states require magnetic-anisotropy to support finite critical currents. See E. Cornfeld, M. S. Rudner, and E. Berg, Spin-polarized superconductivity: Order parameter topology, current dissipation, and multiple-period Josephson effect, Phys. Rev. Research **3**, 013051 (2021). Spin-orbit coupling of graphene sheets is weak, but likely strong enough to limit the impact of spin-rotation supercurrent decay channels. For estimates of spin-orbit coupling strengths in graphene see S. Konschuh, M. Gmitra and J. Fabian, Phys. Rev. B. **82**, 245412 (2010) and J. C. Boettger and S. B. Trickey, Phys. Rev. B. **75**, 121402(R) (2007).

[49] F. Wu and S. Das Sarma, Identification of superconducting pairing symmetry in twisted bilayer graphene using in-plane magnetic field and strain, Phys. Rev. B **99**, 220507(R) (2019).

[50] R. Bistritzer and A. H. MacDonald, Moiré bands in twisted double-layer graphene, Proceedings of the National Academy of Sciences **108**, 12233 (2011).

[51] Y. H. Kwan, S. A. Parameswaran, and S. L. Sondhi, Twisted bilayer graphene in a parallel magnetic field, Phys. Rev. B **101**, 205116 (2020).

[52] S. Carr, S. Fang, Z. Zhu, and E. Kaxiras, Exact continuum model for low-energy electronic states of twisted bilayer graphene, Phys. Rev. Research **1**, 013001 (2019).

[53] Z. A. H. Goodwin, F. Corsetti, A. A. Mostofi, and J. Lischner, Attractive electron-electron interactions from internal screening in magic-angle twisted bilayer graphene, Phys. Rev. B **100**, 235424 (2019).

[54] J. M. Pizarro, M. Rösner, R. Thomale, R. Valentí, and T. O. Wehling, Internal screening and dielectric engineering in magic-angle twisted bilayer graphene, Phys. Rev. B **100**, 161102(R) (2019).

[55] Y. W. Choi and H. J. Choi, Dichotomy of electron-phonon coupling in graphene moiré flat bands, arXiv:2103.16132 (2021).

[56] D. J. Scalapino, A common thread: The pairing interaction for unconventional superconductors, Rev. Mod.

Phys. **84**, 1383 (2012).

[57] Valley-singlet spin-triplet pairing in the continuum model envelope function description we employ corresponds to microscopic f-wave pairing since inequivalent valleys (on which $\Delta(\boldsymbol{k})$ has opposite sign) are related by 60 degree rotations.

[58] M. S. Scheurer and R. Samajdar, Pairing in graphene-based moiré superlattices, Phys. Rev. Research **2**, 033062 (2020).

[59] A. Uri, S. Grover, Y. Cao, J. A. Crosse, K. Bagani, D. Rodan-Legrain, Y. Myasoedov, K. Watanabe, T. Taniguchi, P. Moon, M. Koshino, P. Jarillo-Herrero, and E. Zeldov, Mapping the twist-angle disorder and Landau levels in magic-angle graphene, Nature **581**, 47 (2020).

[60] H. C. Po, L. Zou, A. Vishwanath, and T. Senthil, Origin of Mott insulating behavior and superconductivity in twisted bilayer graphene, Phys. Rev. X **8**, 031089 (2018).

[61] M. Xie and A. H. MacDonald, Nature of the correlated insulator states in twisted bilayer graphene, Phys. Rev. Lett. **124**, 097601 (2020).

[62] F. Guinea and N. R. Walet, Electrostatic effects, band distortions, and superconductivity in twisted graphene bilayers, Proceedings of the National Academy of Sciences **115**, 13174 (2018).

[63] E. Lake and T. Senthil, Re-entrant superconductivity through a quantum Lifshitz transition in twisted trilayer graphene, arXiv:2104.13920 (2021).